Nuclear Science and Techniques (2026) 37:35
https://doi.org/10.1007/s41365-025-01841-x

Process analysis of nuclear hydrogen production via intermediate temperature SOEC electrolysis

Qing Shao[1,2] · **Yue Lu**[2] · **Dun Jin**[2] · **Ling-Hong Luo**[1] · **Xiu-Lin Wang**[3] · **Hui-Chao Yao**[3] · **Ruo-Yun Dai**[3] · **Cheng-Zhi Guan**[2,4,5] · **Guo-Ping Xiao**[2,4] · **Jian-Qiang Wang**[4,5]

Received: 17 July 2024 / Revised: 21 August 2024 / Accepted: 21 September 2024 / Published online: 5 January 2026

Abstract

When the operating temperature of a solid oxide electrolysis cell (SOEC) is lower than the outlet temperature of a nuclear reactor, the reactor can be directly coupled with the SOEC as a high-temperature heat source. However, the key to the efficiency and return on investment of this hybrid energy system lies in the expected lifetime of the SOEC. This study assessed Ni-YSZ|YSZ|GDC|LSC fuel electrode support cells' long-term stability during electrolysis at 650 °C with a current density of $-0.5\ \mathrm{A\ cm^{-2}}$ over 1818 h. The average voltage degradation rate of $2.63\%\ \mathrm{kh^{-1}}$ unfolded in two phases: an initial rapid decay (90 to 1120 h at $3.58\%\ \mathrm{kh^{-1}}$) and a stable decay (1120 to 1818 h at $2.14\%\ \mathrm{kh^{-1}}$), emphasizing SOECs' probability coupling with nuclear reactors at 650 °C. Post-1818-hour electrolysis revealed nickel particle formation associated with $\mathrm{Ni(OH)}_x$ diffusion and re-deposition, alongside a strontium-containing layer causing interface cracking. Despite minimal strontium segregation in the EDS, XPS data indicated surface segregation of Sr. This study provides crucial insights into prolonged SOEC operation, highlighting both its potential and challenges.

Keywords Nuclear hydrogen production · SOEC · Stability · Intermediate temperature

1 Introduction

The rising global demand for energy, coupled with ambitious decarbonization targets, has catalyzed a significant shift toward more sustainable energy systems. As traditional energy sources increasingly fall out of favor owing to their environmental impacts, the spotlight has turned to more sustainable alternatives that promise not only reduced carbon footprints, but also robust reliability and scalability [1, 2]. Among these, nuclear power is particularly promising. Unlike many renewable energy sources, which are often

---

Qing Shao and Yue Lu contributed equally to this work.

This work was supported by the Strategic Priority Research Program of the Chinese Academy of Sciences (No. XDA0400000), the Youth Innovation Promotion Association of the Chinese Academy of Sciences (No. 2021253), the Major Science and Technology Projects of China National Offshore Oil Corporation Limited during the 14th Five Year Plan (No. KJGG-2022-12-CCUS-030500) and the Photon Science Center for Carbon Neutrality of Chinese Academy of Science.

✉ Ling-Hong Luo
luolinghong@tsinghua.org.cn

✉ Cheng-Zhi Guan
guanchengzhi@sinap.ac.cn

✉ Guo-Ping Xiao
xiaoguoping@sinap.ac.cn

✉ Jian-Qiang Wang
wangjianqiang@sinap.ac.cn

[1] School of Materials Science and Engineering, Jingdezhen Ceramic University, Jingdezhen 333403, China

[2] Department of Hydrogen Technique, Shanghai Institute of Applied Physics, Chinese Academy of Sciences, Shanghai 201800, China

[3] CNOOC Gas and Power Group/R & D center, Beijing 100020, China

[4] Key Laboratory of Interfacial Physics and Technology, Chinese Academy of Sciences, Shanghai 201800, China

[5] Shanghai Hyenergy Technology Co., Ltd., Shanghai 201800, China

intermittent, such as solar and wind energy, nuclear power offers a steady and reliable flow of energy [3, 4]. Moreover, it does so without the direct emission of greenhouse gases, which are a major contributor to climate change [5]. The role of nuclear energy extends beyond simply providing electricity. It is increasingly regarded as a versatile player in the energy sector, capable of supporting various industrial processes through the generation of combined heat and power [6]. The multipurpose utility of nuclear energy is crucial in the broader context of creating more integrated and efficient energy systems. One of the most significant aspects of nuclear energy's potential in the modern energy landscape is its ability to produce hydrogen [7].

Hydrogen is increasingly viewed as a critical element for transitioning to a sustainable energy future. It serves as a clean energy carrier, an effective solution for energy storage, and a valuable feedstock for numerous industrial processes [8–10]. Producing hydrogen through nuclear power not only satisfies the energy system's need for low-carbon solutions, but also aligns with global efforts to establish a more sustainable, reliable, and diversified energy supply chain [11].

To harness this potential effectively, advanced nuclear reactor technologies, such as very high-temperature reactors (VHTR), supercritical water reactors (SCWR), and molten salt reactors (MSR), have been developed. These reactors are designed to provide the high-temperature heat necessary for efficient large-scale industrial applications, including hydrogen production [12]. The VHTR is notable for its use of helium as a coolant, which allows it to reach temperatures exceeding 1000 °C. Such high temperatures make VHTRs ideal for thermochemical hydrogen production, a process that can split water into hydrogen and oxygen at high efficiencies [13, 14]. Meanwhile, intermediate-temperature reactors, which operate at lower temperatures than VHTRs, can still play a pivotal role in hydrogen production through technologies such as solid oxide electrolysis cells (SOEC) [7, 15]. SOECs are a compelling technology for hydrogen production, capable of leveraging both electrical and thermal energy produced by nuclear reactors. These cells operate more efficiently at higher temperatures, which enhance their reaction kinetics, making them a promising option for sustainable hydrogen production [16]. In recognition of their potential, the European Union has funded numerous projects under the Hydrogen Joint Undertaking (FCH-JU) to advance SOEC technology and integrate it with existing energy systems [17, 18].

Research on SOECs and their integration with nuclear power has been ongoing for several years. In 2003, the Idaho National Laboratory initiated a significant project to explore the possibilities of hybrid nuclear energy systems incorporating SOECs [19, 20]. Various studies have examined system efficiencies under different operational conditions and system setups. For instance, Peters et al. [21] examined the efficiencies of SOEC systems when they were integrated with external heat sources. Their findings indicated that efficiencies could vary from 90% to 104%, depending on the configuration and operation of the system. Similarly, Milewski et al. [22] explored the integration of protonic and ionic SOECs with nuclear reactors, calculating the energy consumption for hydrogen production to be 38.83 and 37.55 $\mathrm{kWh\,kg^{-1}}$, respectively, which they found to be significantly efficient. Further studies, such as those by Fütterer et al. [23] within the European GEMINI+ project, have examined the coupling of high-temperature gas-cooled reactor (HTGR) power plants with SOECs. Their research suggested that extending the service life of SOECs could significantly enhance the feasibility and efficiency of such hybrid energy systems. Yalamati et al. [24] posited that the efficiency of SOECs depends on the nuclear heat source used. They suggested that utilizing both electricity and waste heat from nuclear power plants could elevate the hydrogen production efficiency of SOECs to as much as 60%. Moreover, Zhang et al. [25] calculated the thermo-hydrogen conversion efficiency for different coupling methods, finding when all the heat for SOECs is provided by a nuclear reactor, the highest thermo-hydrogen conversion efficiency is achieved with the nuclear reactor's outlet temperature at 900 °C.

Most research has been focused on anode-supported and electrolyte-supported SOECs operating at temperatures above 750 °C, whereas the outlet temperature of the MSR is as follows 700 °C [26]. Considering that direct coupling offers significant advantages for large-scale hydrogen production, the outlet steam temperature of the nuclear reactor should exceed the operating temperature of the SOEC [25]. In this situation, acting as a high-temperature heat source, nuclear waste heat can be used for heating the SOEC module, gas preheating, and water vaporization processes [4]. To align with the outlet temperature of the MSR, the working temperature of the SOEC should be lowered to a medium temperature range, approximately 650 °C.

Although when SOEC operation is advantageous at high temperatures (> 800 °C), it can introduce challenges [27]. One of the primary issues at these temperatures is the mutual diffusion of the components within the electrolysis cell. High temperatures can cause materials within the cell to intermingle at the molecular level, potentially leading to degradation of the cell's structural integrity over time. This can result in a loss of efficiency and shorter operational lifespan of the cell. In addition, particle aggregation is a significant concern. At high temperatures, the particles within the cell materials can start to clump together, which can affect the cell performance by altering the material properties crucial for efficient operation. Another significant challenge is the selection of appropriate sealants. Sealants play a critical role in maintaining the integrity of SOECs by ensuring that the separate components of the cell are adequately sealed and do not leak. At high temperatures, finding materials that can withstand heat and maintain a robust seal is difficult. Many commonly used sealant materials either degrade or lose their sealing properties at high temperatures, posing a substantial challenge to maintenance of the overall effectiveness and safety of the system. In response to these high-temperature challenges, there has been a shift in focus toward developing intermediate-temperature SOECs (IT-SOECs) operating at approximately 650 °C. IT-SOECs offer a promising alternative that significantly mitigates the issues associated with high-temperature operations. Lower to medium temperatures impose reduced demands on connectors and seals in the fuel cell stack, aligning with the trend toward mid- to low-temperature transformation of SOEC [28].

Considering that the efficiency and return on investment of hybrid energy systems are constrained by the short service life of SOECs, investigating the long-term stability of SOECs at intermediate temperatures is crucial. The objective of this study is to reveal the alterations in the electrochemical behavior of the cell through stability tests on commercial Ni-YSZ|YSZ|GDC|LSC planar cells, specifically targeting electrolysis at 650 °C. Through the voltage-over-time curve and post-testing microscopic analysis, the degradation mechanisms within various components of the cell under intermediate temperatures were explored. Extensive research and development in this field highlight the synergy between nuclear power and hydrogen production as a beacon of hope for a more sustainable energy future. By leveraging advanced nuclear technologies and innovative hydrogen production methods, such as SOECs, we can move closer to achieving a low-carbon, high-efficiency energy system that not only meets global energy demands, but also adheres to stringent environmental standards.

2 Experimental

2.1 Description of the hybrid energy system

The schematic depicted in Fig. 1 illustrates a nuclear-powered hydrogen production system in which the primary energy source is the MSR. In this system, the coolant salt heated in the MSR core is directed into a heat exchanger. This is a crucial step because the heat exchanger plays a pivotal role in transferring the immense thermal energy carried by the coolant salt to other parts of the system. Following the heat exchange process, thermal energy facilitates electricity generation via a turbine and generator setup. The electricity produced is then strategically distributed to serve two purposes. First, a portion of this electricity is fed into the electrical grid, contributing to the general power supply. Second, the remaining electricity is specifically allocated to power SOECs, which are tasked with the electrolysis of water, a key step in hydrogen production. Additionally, this electricity ensures the smooth functioning of various system components, including pumps, separators, and compressors,

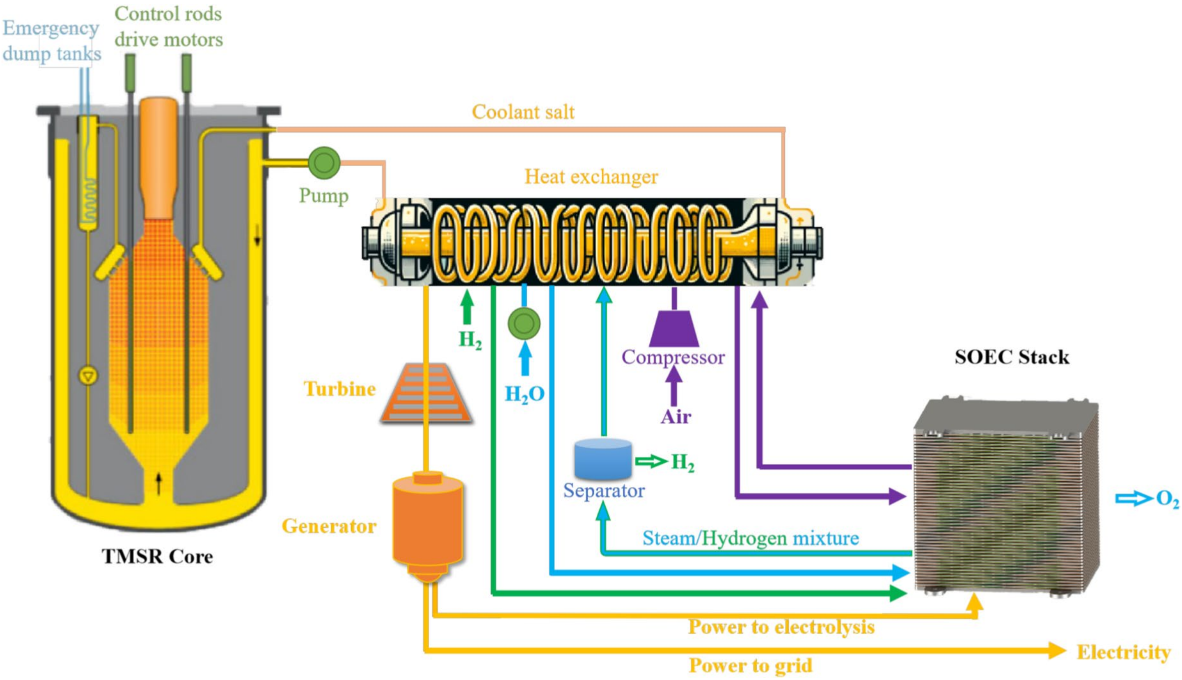

Fig. 1 Schematic of the nuclear-powered hydrogen production system

which are essential for maintaining operational continuity and system integrity of the system.

The exchanged heat is utilized for heating the SOEC module, gas preheating, and water vaporization processes, all of which are essential in the hydrogen production pathway. Notably, the gas produced by the SOEC still possesses a high heat value, which is subsequently released to processes such as water vaporization through another heat exchanger, a step that is simplified in the diagram. The repurposing of waste heat significantly enhances the thermal efficiency of the system.

In the system shown in Fig. 1, the heating of the SOEC module, water vaporization, and gas superheating are powered by waste heat from the MSR. Within this framework, only the electricity required for the operation of the SOEC for water electrolysis (p_{ele}) and the power needed to run other components, such as pumps and compressors (p_{other}), are supplied by the electricity generated by the MSR. This design effectively utilizes the thermal energy of the MSR for process heating, thereby optimizing the energy efficiency of the system by repurposing waste heat for critical thermal processes, while relying on the MSR-generated electricity for operations that require it. This integrated approach enhances the overall energy efficiency and sustainability of the hydrogen production process, and the corresponding efficiency is calculated as Eq. (1) [25]:

$$\eta = \frac{m \cdot \text{HHV}}{p_{\text{ele}} + p_{\text{other}}}, \tag{1}$$

where m is the mass flow rate of produced hydrogen, and HHV is the high-heat value of hydrogen (HHV =285.8 kJ mol^{-1}). The HHV includes the energy released from both the combustion of hydrogen to form water and the subsequent condensation of water vapor into liquid water.

2.2 The cell and the test system

In this study, the examination was carried out on commercial fuel electrode-supported cells, with detailed specifics on cell preparation documented in preceding articles [16]. As presented in Fig. 2, a detailed exploration of the cell cross-sectional microstructure was performed using scanning electron microscopy (SEM), providing a comprehensive understanding of the material interfaces and layer continuity, which are essential for optimizing cell performance. At the bottom is a support layer for the fuel electrode, typically comprising approximately 400 μm of Ni/3YSZ (yttria-stabilized zirconia). The substantial thickness of approximately 400 μm ensures mechanical robustness, allowing the cell to withstand the stresses encountered during operation at elevated temperatures and the dynamic conditions of electrolysis. This support layer is complemented by an active fuel electrode layer, featuring a Ni/8YSZ composition with a thickness of approximately 12 μm. A thinner active fuel electrode layer is tailored for enhanced catalytic activity and increased ionic conductivity, which are crucial for the electrolysis process. An in-depth analysis further reveals the presence of a 3 μm electrolyte layer, the very thin electrolyte is critical for maintaining high ionic conductivity while ensuring minimal electronic leakage. The thinness of the layer substantially reduces the ohmic losses, which ensures the attainment of high current densities at the relatively lower operational temperature of 650 °C. This is followed by a 3 μm gadolinium-doped ceria (GDC) barrier layer, which plays an integral role in mitigating chemical reactivity and inter-diffusion issues between the YSZ electrolyte and the $La_{0.6}Sr_{0.4}CoO_{3-\delta}$ (LSC) oxygen electrode. GDC was chosen for its excellent ionic conductivity and chemical compatibility with both YSZ and LSC. This layer aids in stabilizing the triple-phase boundary (TPB), where electrochemical reactions occur, thus enhancing the overall efficiency and longevity of the cell. Additionally, the cell comprises a 12 μm LSC (lanthanum strontium cobaltite) oxygen electrode, which is noteworthy for its compatibility with intermediate-temperature operations compared to other oxygen electrode materials. The cell dimensions were 5 cm ×5 cm, with the air electrode measuring 4 cm ×4 cm. With an active area of 16 cm^2, the cell provides meaningful data for industrial application scenarios.

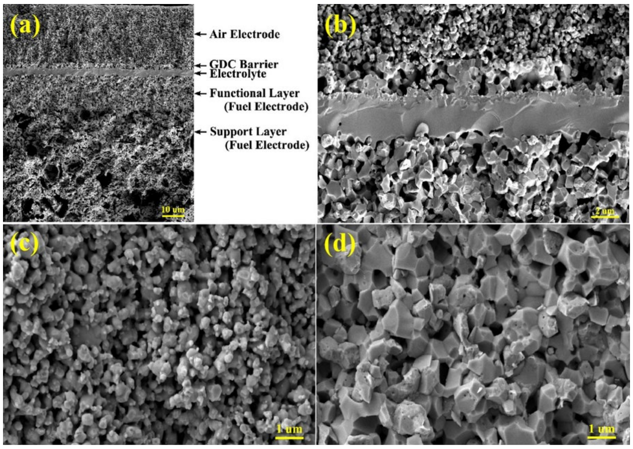

Fig. 2 Cross-sectional SEM images of the electrolysis cell [16]

To align with the outlet temperature of the molten salt nuclear reactor, which is below 700 °C [26], the operating temperature of the SOEC was reduced to approximately 650 °C. Consequently, in this study, we placed the electrolysis cell in a furnace set to 650 °C to simulate the coupling of the SOEC with the MSR. The electrochemical performance of the cell was evaluated using a custom-designed integrated testing station. As shown in Fig. 3, this setup was meticulously engineered to provide a highly controlled

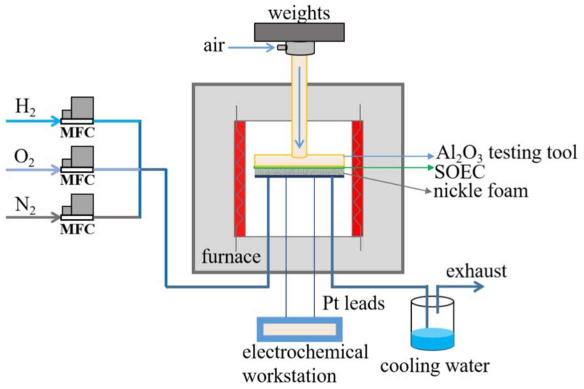

Fig. 3 The single-cell testing set-up of steam electrolysis

environment, essential for achieving reproducible and precise electrochemical measurements. The gas supply system is critical because it manages the feed gases of both electrodes (typically hydrogen, steam, and air) involved in the electrolysis process. The precision in controlling these gas flows was achieved using high-quality mass flow controllers, which are essential for maintaining the desired gas compositions and ratios. The gas composition for the fuel electrode in our experiments was 80% steam and 20% hydrogen. Specifically, the flow rates were 230 ml min^{-1} for steam and 58 ml min^{-1} for hydrogen, with hydrogen serving as a protective gas to prevent Ni oxidation. On the oxygen electrode side, pure air was supplied at a flow rate of 1152 ml min^{-1}. The core of the testing station is its ability to perform various electrochemical tests, such as electrochemical impedance spectroscopy (EIS), current–voltage (*I*–*V*) measurements, and durability testing. These tests are instrumental in evaluating cell performance under different operational conditions. In addition, accurate temperature control via a thermal management system is indispensable. The design of this testing system ensures the reliability and reproducibility of the electrolysis process, as detailed in previous studies [16].

2.3 The cell and the test system

Experimental assessments involved current–voltage polarization curves to explore the initial performance of the cell. The fuel electrode was supplied with a steam content of 80%, while the operating temperature was varied between 600, 650, 700, and 750 °C to investigate the temperature's impact on SOEC performance. Stability testing over prolonged periods is crucial for understanding the operational viability of SOEC in specific applications. Subsequently, a current density of –0.5 A cm^{-2} was applied to the cell at a temperature of 650 °C to explore its stability. The steam content was maintained at 80%, and this steam partial pressure was considered to increase the cell voltage and gas diffusion impedance [29, 30].

To gain insights into the degradation mechanism of the electrolysis cell, post-test characterization was performed. Scanning electron microscopy (SEM, Carl Zeiss, Germany) and energy-dispersive spectrometry (EDS, Zeiss Merlin Compact, Germany) were employed to analyze the microstructure and composition of the cell denoted as "aging cell," which was subjected to a stability test for 1800 h. SEM analysis provided detailed insights into the morphological changes that occurred during long-term operation. EDS analysis further complemented these findings by revealing compositional shifts, such as the depletion of active elements and the formation of secondary phases, which could negatively affect the electrochemical performance of the cell. A reference electrolysis cell from the same production batch, subjected only to reduction, served as a comparison point. The reference cell maintained its original microstructural and compositional integrity during cycling. Comparing the aging cell with the reference specimen allowed for a clearer understanding of the degradation processes, thereby highlighting the extent of degradation in the aged cell.

3 Results and discussion

3.1 Initial performance and evolution of the cell

The initial experiments, conducted through current–voltage (*I*–*V*) polarization tests, as depicted in Fig. 4a, provided crucial data on the electrochemical behavior of the SOEC under operational conditions. These tests serve to establish a baseline from which the durability and long-term stability of the cells can be assessed. The current–voltage (*I*–*V*) polarization curves were tested under a steam flow rate of 230 ml min^{-1} at the fuel electrode and 1152 ml min^{-1} of air at the air electrode. The cell's performance varied across a temperature range from 600 to 750 °C, demonstrating an inverse relationship between temperature and the open circuit voltage, coherent with the predictions from the Nernst equation, which could be formulated as [31]:

$$E = E_0 - \frac{RT}{2F} \ln \left(\frac{P_{H_2O}}{P_{H_2} \cdot \sqrt{P_{O_2}}} \right). \tag{2}$$

Here, E_0 represents the theoretical voltage in the standard state, which is also known as the Nernst electromotive force. R is the gas constant, T is the absolute temperature, and F is Faraday's constant. The number of electrons transferred in the reaction is 2. P_{H_2O} and P_{H_2} represent the partial pressures of steam and hydrogen in the fuel electrode, respectively,

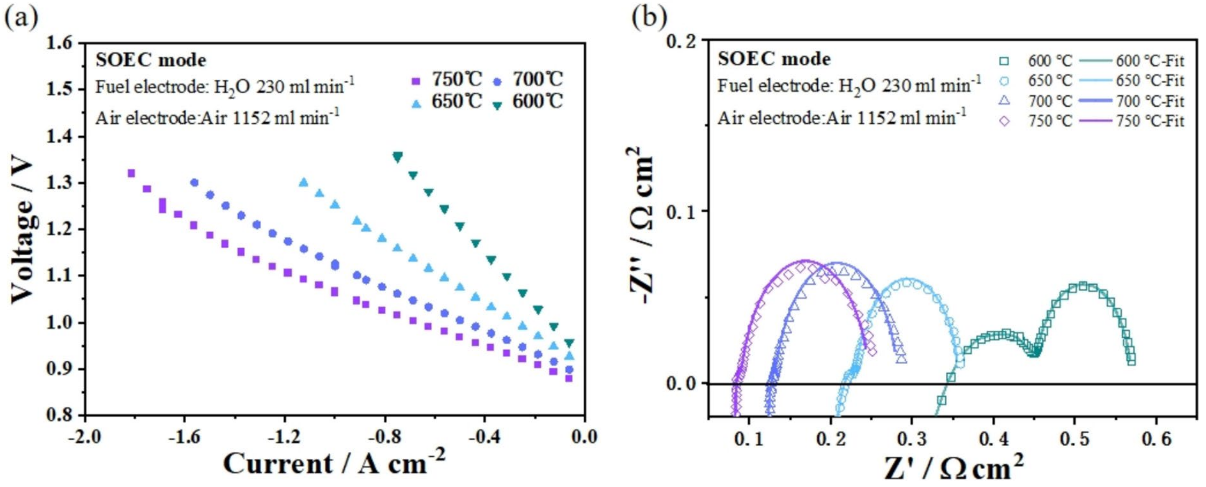

Fig. 4 **a** The initial *I*–*V* curves and **b** the EIS spectra at different temperatures in SOEC modes

and P_{O_2} represents the oxygen partial pressure in the air electrode.

At higher temperatures of 750 °C and 700 °C, the *I*–*V* curves showed current limitations, where the voltage increased disproportionately relative to the current density, indicating nonlinear characteristics. This behavior, specifically the turning points at a steam conversion of 48.48%, is likely due to concentration polarization caused by limitations in gas diffusion [31]. At these higher operational temperatures, the kinetic processes may be enhanced, but the physical transport of reactants to the three-phase boundary (TPB) becomes a limiting factor.

Although the electrolysis cell could attain a higher electrolysis current density and hydrogen production efficiency at elevated temperatures. In this study, a temperature of 650 °C was chosen to align with the temperature range associated with nuclear reactor outlet temperatures. At 650 °C, the *I*–*V* curve showed a linear relationship, suggesting an adequate gas supply for efficient electrolysis.

Figure 4b shows the electrochemical impedance spectroscopy (EIS) results at different temperatures and provides critical insights into how temperature affects the cell efficiency. The data show that lower temperatures increase both the Ohmic and Polarization impedances within the electrolysis cell. This is attributed to the pronounced effects of temperature on oxygen ion transport kinetics within the electrolyte, the catalytic effectiveness of nickel (Ni), and the charge transfer dynamics at the TPB [32, 33]. Temperature significantly influences the mobility of oxygen ions in the electrolyte. Lower temperatures tend to slow down the kinetics, leading to higher impedance as the ionic conductivity decreases at lower temperatures. Furthermore, Nickel, which is commonly used as a fuel electrode material in SOECs, exhibits decreased catalytic activity at lower temperatures. This reduction in activity impairs the overall efficiency of the electrochemical reactions, particularly the hydrogen evolution reaction. The TPB, where the electrolyte, electrode, and gas phase meet, is crucial for effective charge transfer. At lower temperatures, the charge transfer dynamics are hindered, contributing to an increase in the polarization impedance.

The specific values reported, such as the Ohmic impedance of 0.22 Ω and polarization impedance of 0.14 Ω at 650 °C highlight the more favorable conditions at this temperature compared to lower temperatures like 600 °C, where a significantly increased impedance arc is noted for the charge transfer reaction at the fuel electrode. This suggests that 650 °C may be more suitable for long-term stability research of the cell, as it provides better conductivity and catalytic activity at the temperature window for coupling SOEC with MSR, minimizing the losses associated with impedance, and enhancing overall cell performance.

The long-term stability of solid oxide electrolysis cells (SOECs) is crucial for their practical application, particularly in coupling with nuclear energy systems for hydrogen production. Figure 5 presents the voltage–time (*V*–*T*) curve of the SOEC operating in the galvanostatic mode, offering insights into its performance and degradation behavior over an extended period. The stability test was conducted at −8 A (−0.5 A cm^{-2}) and 650 °C, with the same atmosphere as the initial performance test. The electrolysis cell demonstrated stable operation in the SOEC mode for more than 1800 h. The *V*–*T* curve can be divided into three distinct phases, each characterized by a different degradation rate. During the initial 90 h, the curve fitting of voltage versus time yielded a slope of approximately -3.604×10^{-5}, indicating a degradation rate of −3.42% kh^{-1} over this period. The negative slope indicates a decrease in degradation,

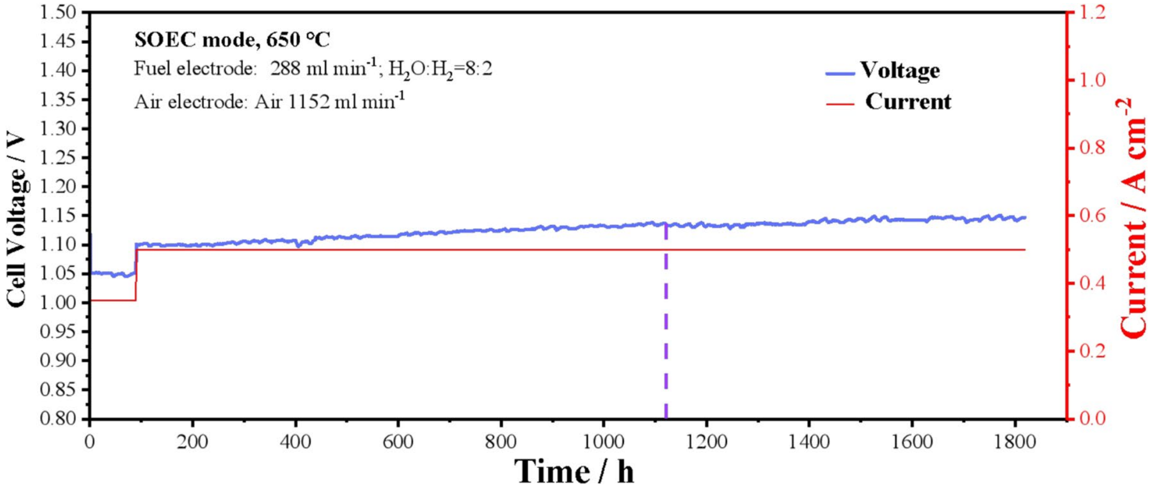

Fig. 5 The long-term *V*–*T* curve of the SOEC at 650 ℃

suggesting an activation process in which the cell components stabilize and improve their performance [33]. In the following phase, spanning from 90 h to 1120 h, the voltage of the electrolysis cell increased from 1.101 V to 1.136 V, representing a linear degradation rate of approximately 3.58% kh^{-1}. This phase is marked by a rapid decay process, reflecting a period of significant degradation, as reported by Wang et al. [16, 34]. Throughout the steady decay period from 1120 h to 1818 h, the voltage of the electrolysis cell continued to increase, although at a slower rate than that in the previous phase. The average degradation rate during this phase was calculated to be 2.14% kh^{-1}. The reduction in the slope of the voltage curve indicates a transition to a more stable degradation phase. This steady decay period aligns with the patterns reported in Ref. [35], characterized by a slower, more consistent rate of degradation. Consequently, the long-term stability exhibited by the SOEC in this study suggests substantial potential for its use in coupling with nuclear energy systems for water electrolysis applications. The relatively low degradation rates, especially during the steady decay phase, indicate that SOECs can maintain their efficiency over extended periods, making them suitable for continuous hydrogen production applications.

3.2 Post-test analysis of cells

In studies of SOEC operating at intermediate temperatures, one critical aspect is understanding the factors contributing to cell degradation. To this end, SEM and EDS were employed to analyze the microstructure and elemental distribution of the tested cells. This approach enabled a comprehensive examination of both the physical and chemical changes occurring in the fuel electrode over time. Figure 6 presents cross-sectional SEM images, depicting the morphology of the SOEC before and after stability testing. In contrast to the blocky structure of Ni-YSZ shown in Fig. 6a,

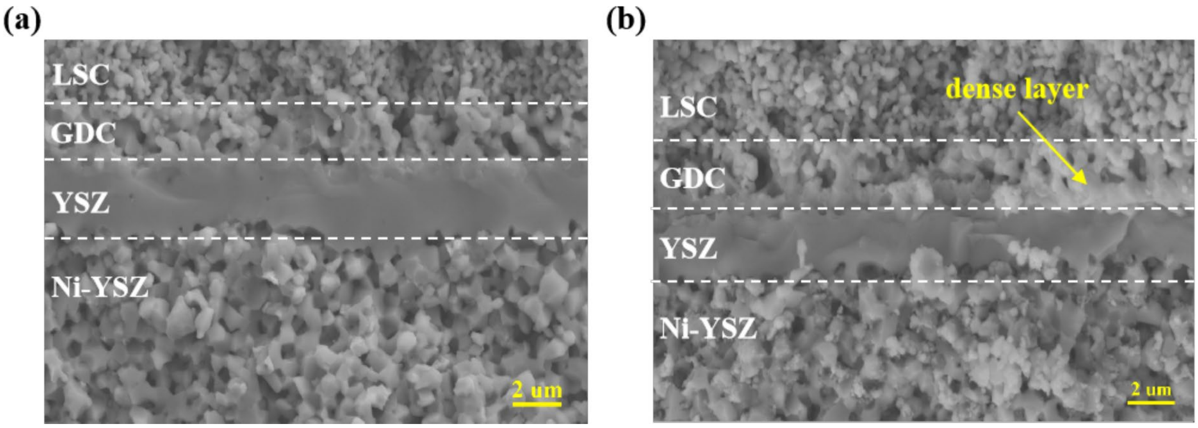

Fig. 6 Cross-sectional SEM images of the SOEC **a** before and **b** after operation

significant microstructural changes were observed in the Ni-YSZ layer after long-term testing (Fig. 6b). Within the Ni-YSZ functional layer of the post-testing fuel electrode, numerous particles with a diameter of approximately 100 nm were observed near the electrolyte interface. The presence of these particles indicates significant microstructural alterations that could impact the overall performance and stability of SOECs [36, 37]. Additionally, the SEM images highlighted the presence of microcracks and voids between the electrolyte layer and the GDC barrier. These defects can impede ionic conductivity and exacerbate degradation processes, leading to a further decline in cell efficiency [38]. Furthermore, the dense layer found between the electrolyte layer and GDC barrier layer may be indicative of secondary phase formation, possibly resulting from interactions between the electrode materials and electrolyte. These phases could contribute to degradation by introducing additional resistive interfaces within the cell, thus impacting the overall electrochemical performance [39].

Further analysis was conducted on the Ni-YSZ fuel electrode of the cell after long-term stability testing, as shown in Fig. 7. The SEM and EDS results of the Ni-YSZ fuel electrode showed no obvious Ni migration during this process. Ni migration within SOECs is a multifaceted phenomenon influenced by several factors, including the electrolysis current density, electric field strength and distribution caused by Ni distribution, concentration gradients of hydrogen and steam, and temperature gradients [40]. This complex process lacks a definitive mechanistic explanation owing to the interplay of various factors. The absence of pronounced Ni migration despite 1800 operational hours in this study suggests that the conditions within the cell might not have reached the thresholds required for significant Ni migration, or that the migration rate was too slow to be detected. This finding is critical because it indicates that the stability of the Ni-YSZ can be maintained under certain operational conditions, potentially leading to longer cell lifetimes.

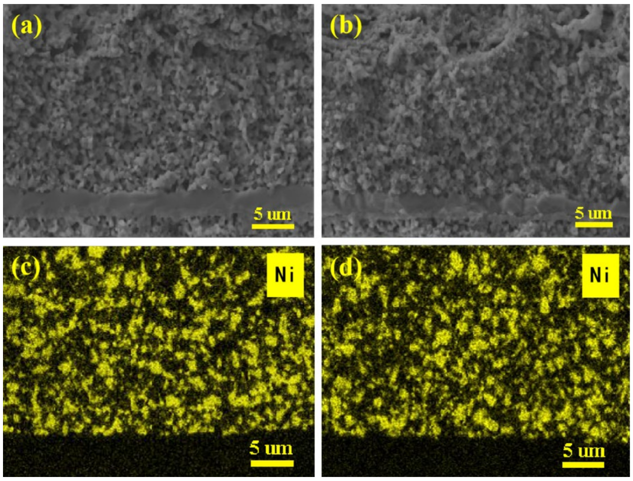

Fig. 7 The SEM and EDS images of the Ni-YSZ fuel electrode **a**, **c** before and **b**, **d** after long-term stability testing

EDS analysis revealed the presence of minute nickel-containing particles, as evidenced by the EDS mapping results shown in Fig. 8. Mogensen et al. [41, 42] attributed the migration dynamics of nickel (Ni) to the generation of $Ni(OH)_x$ volatile species diffusing by the vapor pressure gradient. Specifically, under conditions of elevated water vapor pressure (P_{H_2O}) above 80%, nickel reacts with water, resulting in higher concentrations of $Ni(OH)_x$, where x can be either 1 or 2. In the SOEC mode, the current is driven by an external power source, flowing from the oxygen electrode through the electrolyte to the fuel electrode. The fuel electrode is typically supplied with a gas mixture rich in water vapor, such as steam combined with a small amount of hydrogen. The steam is electrolyzed at the electrode into hydrogen and oxygen ions, with $x = 1$ being predominant in this scenario. Conversely, in the SOFC mode, the current is driven by the chemical energy of the fuel, which flows from the fuel electrode to the oxygen electrode. The fuel electrode is provided with a fuel gas, such as pure hydrogen, which reacts with oxide ions at the electrode, releasing electrons and producing water as a byproduct. In this scenario, $x = 2$ becomes dominant. Consequently, $Ni(OH)_x$ diffuses from high concentration to lower concentration, along the concentration gradient, and is consistent with the decreasing direction of P_{H_2O}. As a result, $Ni(OH)_x$ diffused from the interface between the electrolyte and the fuel electrode toward the interior of the fuel electrode in the SOFC mode. Conversely, in the SOEC mode, diffusion occurs from the support layer to the interior of the fuel electrode. This migration of $Ni(OH)_x$ is driven by the reactions outlined in Eqs. (3) and (4), wherein nickel is generated and subsequently deposited, contributing to Ni migration. In this investigation,

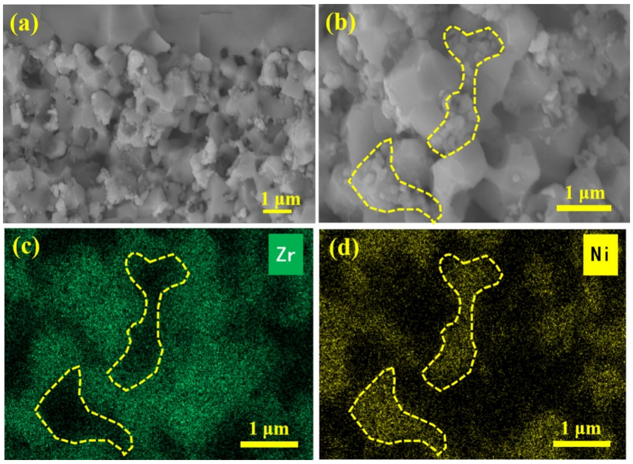

Fig. 8 SEM and EDS analysis of Ni-YSZ fuel electrode after electrolysis

an electrolysis cell was subjected to an SOEC operational environment for 1818 h. Although the EDS results in Fig. 7 indicate a lack of significant Ni migration, the observation of numerous small Ni particles within the functional layer of the fuel electrode suggests the possibility of $Ni(OH)_x$ species undergoing diffusion and subsequent re-deposition.

$$\begin{aligned} &Ni(OH)_x(g) + 2xe^- \ (Ni) \\ &\quad \leftrightarrow Ni(s) + xO^{2-} \ (YSZ) + \frac{1}{2}xH_2(g) \end{aligned} \tag{3}$$

$$Ni(OH)_x(g) + \frac{1}{2}xH_2(g) \leftrightarrow Ni(s) + xH_2O(g) \tag{4}$$

EDS point scanning of both the small-particle aggregation region and the block-like area, as shown in Fig. 9, provides significant insights into the distribution and migration of Ni within the SOEC structure. The EDS point-scanning results revealed a stark contrast in the Ni content between these regions, with a 6.67% Ni content in the blocky region and a significantly higher 73.56% Ni content in the particle agglomeration area. This analysis provides further support for previous observations and analyses, highlighting the complexity of Ni migration within SOECs and underscoring the need for further research to understand and mitigate Ni migration. By optimizing the operational parameters, conducting in-depth microstructural analyses, and exploring material innovations, the stability and performance of SOECs can be enhanced.

Microstructural analysis of the oxygen electrode post-electrolysis was performed using SEM and EDS. The investigation uncovered changes and potential degradation mechanisms within the SOEC, which could significantly affect its performance and durability. The SEM images shown in Fig. 10 reveal the presence of microcracks at the interface between the oxygen electrode and electrolyte. These cracks undermine the mechanical stability of SOEC and lead to further degradation under operational stresses, accelerating cell degradation [38]. In addition, the SEM images show the formation of a dense layer at the interface, likely resulting from Sr segregation. The dense layer identified through EDS mapping is likely composed of strontium-containing phases, such as $SrZrO_3$. $SrZrO_3$ is an electrical insulator with poor ionic conductivity, measured at 1.87×10^{-6} S cm^{-1} at 800 °C [43]. The formation of the $SrZrO_3$ phase at the electrode/electrolyte interface can obstruct ion migration [44]. Additionally, the diffusion of Sr to the YSZ surfaces results in Sr depletion in the LSC oxygen electrode, promoting the formation of Sr-free $LaCoO_3$, which has significantly reduced electrocatalytic activity for the oxygen reduction reaction (ORR) [45]. The emergence of these Sr-containing high-resistance phases, along with potential electrolyte cracking, is expected to increase the overall resistance of the electrolysis cell [46, 47]. Increased resistance leads to higher energy losses and decreased efficiency, posing significant challenges for long-term operations.

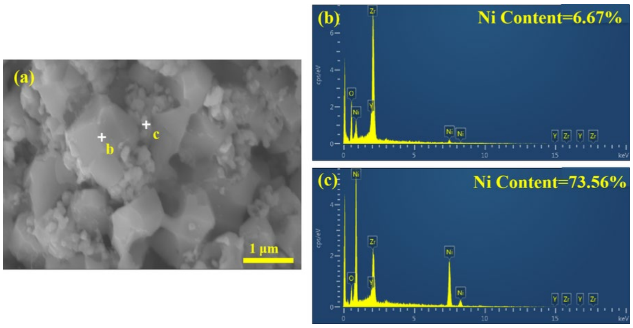

Fig. 9 **a** SEM and **b**, **c** EDS point scanning analysis of Ni-YSZ fuel electrode sections after electrolysis

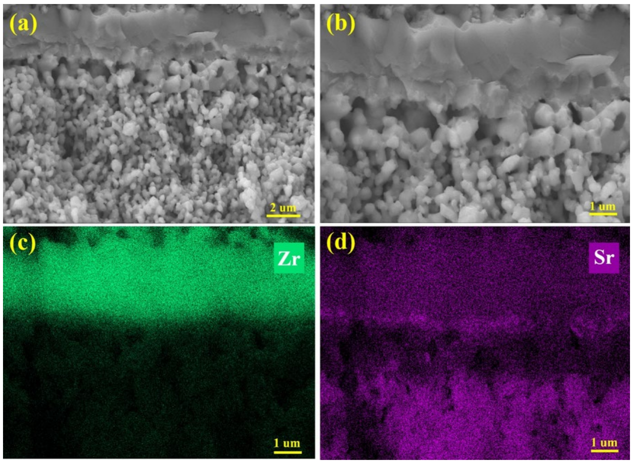

Fig. 10 Observations of microstructural changes in the cells from air electrode using **a**, **b** SEM and EDS mapping of **c** Zr and **d** Sr after electrolysis at −0.5 A cm^{-2}

In the SOEC analysis, EDS mapping indicated that Sr segregation toward the cell surface was not significant. To gain a deeper understanding of the surface chemistry and potential segregation phenomena, XPS was employed to examine the chemical composition and environment, particularly the oxidation state of Sr, in both reference and aged SOECs. The results, depicted in Fig. 11, show the photoelectron spectra of Sr 3d for the two samples, along with the corresponding Sr elemental percentages.

Figure 11a illustrates the fitting results of the Sr 3d peak for the reference cell, whereas Fig. 11b shows the fitting outcomes for the aged sample. The Sr 3d energy level exhibited a dual state. The low binding energy (BE) state of $3d_{\frac{5}{2}}$, indicative of lattice Sr, appeared at approximately 131.9 eV.

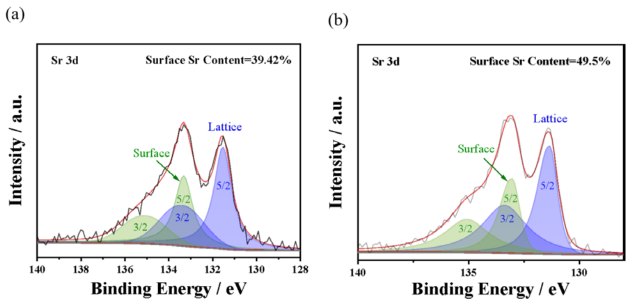

Fig. 11 XPS results of the surface in the cells from the air electrode: **a** the reference sample and **b** the aging sample

The high binding energy state of $3d_{\frac{3}{2}}$, corresponding to the surface Sr, was observed at approximately 133.3 eV [48]. These surface states are speculated to consist of a composite of SrO, $Sr(OH)_2$, and $SrCO_3$ [49, 50]. Quantitative analysis revealed that the proportion of surface Sr to total Sr increased from 39.42% in the reference sample to 49.5% in the aged sample. Quantitative analysis revealed that the proportion of surface Sr to total Sr increased from 39.42% in the reference sample to 49.5% in the aged sample.

This outcome implies that, despite the absence of significant differences in intensity in the EDS mapping, there is an increased tendency for Sr segregation toward the surface of the electrolysis cell after 1818 h of operation.

Sr segregation in LSC electrodes is a well-documented phenomenon, influenced by factors such as material stoichiometry [51], strain [52], temperature [51], oxygen partial pressure [53], LSC microstructure [54], and electrochemical polarization [55]. In this study, the relatively mild electrolysis conditions suggest that Sr segregation to the LSC electrode surface is likely driven by the reaction of Sr with atmospheric CO_2 or H_2O, forming stable compounds such as $SrCO_3$ and $Sr(OH)_2$. These compounds are more stable at the surface, thereby promoting the migration of Sr from the bulk material to the surface [47].

4 Conclusion

To achieve direct coupling between an MSR and SOEC, the robust stability of the SOEC below the outlet temperature of the nuclear reactor is required. Stability tests were conducted on fuel electrode support cells featuring a Ni-YSZ|YSZ|GDC|LSC architecture at 650 °C, employing a current density of $-0.5\ \mathrm{A\,cm^{-2}}$. Throughout the testing period from 90 h to 1818 h, an average voltage degradation rate of $2.63\%\ \mathrm{kh^{-1}}$ was observed. This degradation process unfolded in distinct stages, encompassing an initial rapid decay phase from 90 to 1120 h, characterized by a degradation rate of $3.58\%\ \mathrm{kh^{-1}}$. Subsequently, a stable decay process ensued from 1120 to 1818 h, maintaining a decay rate of $2.14\%\ \mathrm{kh^{-1}}$. These results indicate the viability of SOECs for direct coupling with MSRs at intermediate temperatures, exhibiting a minor voltage degradation rate at 650 °C and demonstrating commendable long-term stability.

Following an electrolysis duration of 1818 h, minute nickel particles were observed within the Ni-YSZ fuel electrode, possibly associated with the diffusion and subsequent re-deposition of $Ni(OH)_x$. Concurrently, a compact strontium-containing layer formed at the interface between the oxygen electrode and electrolyte, leading to interface microcracking. Although pronounced Sr segregation to the surface was not evident in the EDS analyses, the XPS data calculations revealed a tendency for Sr surface segregation.

To further improve the stability of the cell and enhance the efficiency and economic return of the hybrid energy system, efforts should be focused on mitigating Ni migration in the fuel electrode and preventing Sr segregation in the oxygen electrode. Strategies to address these issues may include optimizing material compositions, refining microstructural designs, and controlling operational parameters to reduce the impact of degradation mechanisms.

Author contributions All authors contributed to the study conception and design. Material preparation, data collection and analysis were performed by Qing Shao, Yue Lu, Dun Jin, Ling-Hong Luo, Xiu-Lin Wang, Hui-Chao Yao, Ruo-Yun Dai, Cheng-Zhi Guan, Guo-Ping Xiao and Jian-Qiang Wang. The first draft of the manuscript was written by Qing Shao, and all authors commented on previous versions of the manuscript. All authors read and approved the final manuscript.

Data availability The data that support the findings of this study are openly available in Science Data Bank at https://cstr.cn/31253.11.sciencedb.j00186.00766 and https://www.doi.org/10.57760/sciencedb.j00186.00766.

Declarations

Conflict of interest Jian-Qiang Wang is an editorial board member for Nuclear Science and Techniques and was not involved in the editorial review, or the decision to publish this article. All authors declare that there are no conflict of interest.

References

1. M.J.B. Kabeyi, O.A. Olanrewaju, Sustainable energy transition for renewable and low carbon grid electricity generation and supply. Front. Energy Res. **9**, 743114 (2022). https://doi.org/10.3389/fenrg.2021.743114
2. S. Chu, A. Majumdar, Opportunities and challenges for a sustainable energy future. Nature **488**, 294–303 (2012). https://doi.org/10.1038/nature11475
3. K. Fernandez-Cosials, R. Vecino, C. Vazquez-Rodríguez, A flexible nuclear energy system using cryptoassets as enablers: economic assessment. Prog. Nucl. Energy **161**, 104735 (2023). https://doi.org/10.1016/j.pnucene.2023.104735

4. T. Cui, J. Zhu, Z. Lyu et al., Efficiency analysis and operating condition optimization of solid oxide electrolysis system coupled with different external heat sources. Energy Convers. **279**, 116727 (2023). https://doi.org/10.1016/j.enconman.2023.116727
5. L. Liu, H. Guo, L. Dai et al., The role of nuclear energy in the carbon neutrality goal. Prog. Nucl. Energy **162**, 104772 (2023). https://doi.org/10.1016/j.pnucene.2023.104772
6. C.P. Marcel, Addressing the global energy problem: perspectives, challenges, and potential solutions. Nucl. Eng. Des. **414**, 112610 (2023). https://doi.org/10.1016/j.nucengdes.2023.112610
7. R. Pinsky, P. Sabharwall, J. Hartvigsen et al., Comparative review of hydrogen production technologies for nuclear hybrid energy systems. Prog. Nucl. Energy **123**, 103317 (2020). https://doi.org/10.1016/j.pnucene.2020.103317
8. D.A. Cullen, K.C. Neyerlin, R.K. Ahluwalia et al., New roads and challenges for fuel cells in heavy-duty transportation. Nat. Energy **6**, 462–474 (2021). https://doi.org/10.1038/s41560-021-00775-z
9. L. Van Hoecke, L. Laffineur, R. Campe et al., Challenges in the use of hydrogen for maritime applications. Energy Environ. Sci. **14**, 815–843 (2021). https://doi.org/10.1039/D0EE01545H
10. M. Chatenet, B.G. Pollet, D.R. Dekel et al., Water electrolysis: from textbook knowledge to the latest scientific strategies and industrial developments. Chem. Soc. Rev. **51**, 4583–4762 (2022). https://doi.org/10.1039/d0cs01079k
11. J. Nowotny, T. Hoshino, J. Dodson et al., Towards sustainable energy. Generation of hydrogen fuel using nuclear energy. Int. J. Hydrogen Energ. **41**, 12812–12825 (2016). https://doi.org/10.1016/j.ijhydene.2016.05.054
12. S. Şahin, H.M. Şahin, Generation-IV reactors and nuclear hydrogen production. Int. J. Hydrogen Energ. **46**, 28936–28948 (2021). https://doi.org/10.1016/j.ijhydene.2020.12.182
13. R. lder, R. Allen, Nuclear heat for hydrogen production: coupling a very high/high temperature reactor to a hydrogen production plant. Prog. Nucl. Energy **51**, 500–525 (2009). https://doi.org/10.1016/j.pnucene.2008.11.001
14. A. Simpson, E. Veron, Assessment of the market opportunities for hydrogen derived from high temperature reactor driven processes. Nucl. Eng. Des. **398**, 111961 (2022). https://doi.org/10.1016/j.nucengdes.2022.111961
15. W.C. Adaleti, E.G. de Souza, S.N.M. de Souza, The potential of hydrogen production from high and low-temperature electrolysis methods using solar and nuclear energy sources: the transition to a hydrogen economy in Brazil. Int. J. Hydrogen Energy **47**, 34727–34738 (2022). https://doi.org/10.1016/j.ijhydene.2022.08.065
16. Q. Shao, D. Jin, Y. Lu et al., Performance evolution analysis of solid oxide electrolysis cells operating at high current densities. Int. J. Hydrogen Energy **57**, 709–716 (2024). https://doi.org/10.1016/j.ijhydene.2024.01.096
17. K.R. Schultz, Production of hydrogen by fusion energy: a review and perspective. Fusion Sci. Technol. **44**, 393–9 (2003). https://doi.org/10.13182/FST03-A366
18. O. Posdziech, K. Schwarze, J. Brabandt, Efficient hydrogen production for industry and electricity storage via high-temperature electrolysis. Int. J. Hydrogen Energy **44**, 19089–101 (2019). https://doi.org/10.1016/j.ijhydene.2018.05.169
19. J.E. O'Brien, M.G. McKellar, E.A. Harvego et al., High-temperature electrolysis for large-scale hydrogen and syngas production from nuclear energy—summary of system simulation and economic analyses. Int. J. Hydrogen Energy **35**, 4808–4819 (2010). https://doi.org/10.1016/j.ijhydene.2009.09.009
20. C.M. Stoots, J.E. O'Brien, K.G. Condie et al., High-temperature electrolysis for large-scale hydrogen production from nuclear energy—experimental investigations. Int. J. Hydrogen Energy **35**, 4861–4870 (2010). https://doi.org/10.1016/j.ijhydene.2009.10.045
21. R. Peters, R. Deja, L. Blum et al., Influence of operating parameters on overall system efficiencies using solid oxide electrolysis technology. Int. J. Hydrogen Energy **40**, 7103–13 (2015). https://doi.org/10.1016/j.ijhydene.2015.04.011
22. J. Milewski, J. Kupecki, A. Szczęśniak et al., Hydrogen production in solid oxide electrolyzers coupled with nuclear reactors. Int. J. Hydrogen Energy **46**, 35765–35776 (2021). https://doi.org/10.1016/j.ijhydene.2020.11.217
23. M.A. Fütterer, R. Pabarcius, S. Hübner et al., Nuclear process heat application options: highlights from the European GEMINI+ project. Nucl. Eng. Des. **396**, 111879 (2022). https://doi.org/10.1016/j.nucengdes.2022.111879
24. H.P.S. Yalamati, R.K. Vij, R. Srivastava, in *Solar-Driven Green Hydrogen Generation and Storage*, ed. by R. Srivastava, J. Chattopadhyay, D.M.F. Santos (Elsevier, 2023), pp. 347–362
25. W. Zhang, B. Yu, J. Xu, Efficiency evaluation of high-temperature steam electrolytic systems coupled with different nuclear reactors. Int. J. Hydrogen Energy **37**, 12060–12068 (2012). https://doi.org/10.1016/j.ijhydene.2012.04.024
26. A. Di Ronco, A. Cammi, S. Lorenzi, Preliminary analysis and design of the heat exchangers for the Molten Salt Fast Reactor. Nucl. Eng. Technol. **52**, 51–58 (2020). https://doi.org/10.1016/j.net.2019.07.013
27. J. Mermelstein, O. Posdziech, Development and demonstration of a novel reversible SOFC system for utility and micro grid energy storage. Fuel Cells **17**, 562–570 (2017). https://doi.org/10.1002/fuce.201600185
28. S.J. Kim, K.J. Kim, A.M. Dayaghi et al., Polarization and stability of La_2 $NiO_{4+\delta}$ in comparison with $La_{0.6}$ $Sr_{0.4}$ $Co_{0.2}$ $Fe_{0.8}$ $O_{3-\delta}$ as air electrode of solid oxide electrolysis cell. Int. J. Hydrogen Energy **41**, 14498–14506 (2016). https://doi.org/10.1016/j.ijhydene.2016.05.284
29. J. Liang, Y. Wang, J. Zhu et al., Investigation on the reaction mechanism of solid oxide co-electrolysis with different inlet mixtures based on the comparison of CO_2 electrolysis and H_2O electrolysis. Energy Convers. **277**, 116621 (2023). https://doi.org/10.1016/j.enconman.2022.116621
30. S.D. Kim, D.W. Seo, A.K. Dorai et al., The effect of gas compositions on the performance and durability of solid oxide electrolysis cells. Int. J. Hydrogen Energy **38**, 6569–6576 (2013). https://doi.org/10.1016/j.ijhydene.2013.03.115
31. A. Mahmood, S. Bano, J.H. Yu et al., Performance evaluation of SOEC for CO_2/H_2O co-electrolysis: considering the effect of cathode thickness. J. CO2 Util. **33**, 114–120 (2019). https://doi.org/10.1016/j.jcou.2019.05.014
32. V. Bilalis, B. Li, H.L. Frandsen et al., The effect of operating temperature on galvanostatic operation of solid oxide electrolysis cells. ECS Trans. **111**, 429 (2023). https://doi.org/10.1149/11106.0429ecst
33. Y. Yang, X. Tong, A. Hauch et al., Study of solid oxide electrolysis cells operated in potentiostatic mode: effect of operating temperature on durability. Chem. Eng. J. **417**, 129260 (2021). https://doi.org/10.1016/j.cej.2021.129260
34. Y. Wang, Z. Lyu, M. Han et al., Initial-stage performance evolution of solid oxide fuel cells based on polarization analysis. ECS Trans. **103**, 1261 (2021). https://doi.org/10.1149/10301.1261ecst
35. T. Lehtinen, M. Noponen, Solid oxide electrolyser demonstrator development at elcogen. ECS Trans. **103**, 1939 (2021). https://doi.org/10.1149/10301.1939ecst
36. A. Hauch, S.D. Ebbesen, S.H. Jensen et al., Solid oxide electrolysis cells: microstructure and degradation of the Ni/Yttria-stabilized zirconia electrode. J. Electrochem. Soc. **155**, B1184 (2008). https://doi.org/10.1149/1.2967331
37. X. Sun, P.V. Hendriksen, M.B. Mogensen et al., Degradation in solid oxide electrolysis cells during long term testing. Fuel Cells **19**, 740–747 (2019). https://doi.org/10.1002/fuce.201900081

38. C.E. Frey, Q. Fang, D. Sebold et al., A detailed post mortem analysis of solid oxide electrolyzer cells after long-term stack operation. J. Electrochem. Soc. **165**, F357 (2018). https://doi.org/10.1149/2.0961805jes
39. V. Subotić, S. Futamura, G.F. Harrington et al., Towards understanding of oxygen electrode processes during solid oxide electrolysis operation to improve simultaneous fuel and oxygen generation. J. Power Sources **492**, 229600 (2021). https://doi.org/10.1016/j.jpowsour.2021.229600
40. L.A. Jolaoso, I.T. Bello, O.A. Ojelade et al., Operational and scaling-up barriers of SOEC and mitigation strategies to boost H_2 production—a comprehensive review. Int. J. Hydrogen Energy **48**, 33017–41 (2023). https://doi.org/10.1016/j.ijhydene.2023.05.077
41. M.B. Mogensen, M. Chen, H.L. Frandsen et al., Ni migration in solid oxide cell electrodes: review and revised hypothesis. Fuel Cells **21**, 415–29 (2021). https://doi.org/10.1002/fuce.202100072
42. M.B. Mogensen, A. Hauch, X. Sun et al., Relation between Ni particle shape change and Ni migration in Ni–YSZ electrodes—a hypothesis. Fuel Cells **17**, 434–41 (2017). https://doi.org/10.1002/fuce.201600222
43. F. Wankmüller, J. Szász, J. Joos et al., Correlative tomography at the cathode/electrolyte interfaces of solid oxide fuel cells. J. Power Sources **360**, 399–408 (2017). https://doi.org/10.1016/j.jpowsour.2017.06.008
44. K. Develos-Bagarinao, H. Yokokawa, H. Kishimoto et al., Elucidating the origin of oxide ion blocking effects at GDC/SrZr(Y)O_3/YSZ interfaces. J. Mater. Chem. A **5**, 8733–43 (2017). https://doi.org/10.1039/C7TA01589E
45. R. Kiebach, W.W. Zhang, W. Zhang et al., Stability of $La_{0.6}\,Sr_{0.4}\,Co_{0.2}\,Fe_{0.8}\,O_3/Ce_{0.9}\,Gd_{0.1}\,O_2$ cathodes during sintering and solid oxide fuel cell operation. J. Power Sources **283**, 151–61 (2015). https://doi.org/10.1016/j.jpowsour.2015.02.064
46. Z. Lu, S. Darvish, J. Hardy et al., $SrZrO_3$ Formation at the interlayer/electrolyte interface during $(La_{1-x}\,Sr_x)_{1-\delta}\,Co_{1-y}\,Fe_y\,O_3$ cathode sintering. J. Electrochem. Soc. **164**, F3097 (2017). https://doi.org/10.1149/2.0141710jes
47. K. Chen, S.P. Jiang, Surface segregation in solid oxide cell oxygen electrodes: phenomena, mitigation strategies and electrochemical properties. Electrochem. Energy Rev. **3**, 730–765 (2020). https://doi.org/10.1007/s41918-020-00078-z
48. E. Mutoro, E.J. Crumlin, H. Pöpke et al., Reversible compositional control of oxide surfaces by electrochemical potentials. J. Phys. Chem. Lett. **3**, 40–44 (2011). https://doi.org/10.1021/jz201523y
49. Z. Cai, M. Kubicek, J. Fleig et al., Chemical heterogeneities on $La_{0.6}\,Sr_{0.4}\,CoO_{3-\delta}$ thin films—correlations to cathode surface activity and stability. Chem. Mater. **24**, 1116–1127 (2012). https://doi.org/10.1021/cm203501u
50. O. Celikbilek, G. Sassone, M. Prioux et al., Long-term tests and advanced post-test characterizations of the oxygen electrode in solid oxide electrolysis cells. ECS Trans. **111**, 211 (2023). https://doi.org/10.1149/11106.0211ecst
51. Y. Chen, H. Téllez, M. Burriel et al., Segregated chemistry and structure on (001) and (100) surfaces of $(La_{1-x}\,Sr_x)_2\,CoO_4$ override the crystal anisotropy in oxygen exchange kinetics. Chem. Mater. **27**, 5436–5450 (2015). https://doi.org/10.1021/acs.chemmater.5b02292
52. X. Liu, L. Zhang, Y. Zheng et al., Uncovering the effect of lattice strain and oxygen deficiency on electrocatalytic activity of perovskite cobaltite thin films. Adv. Sci. **6**, 1801898 (2019). https://doi.org/10.1002/advs.201801898
53. D. Oh, D. Gostovic, E.D. Wachsman, Mechanism of $La_{0.6}\,Sr_{0.4}\,Co_{0.2}\,Fe_{0.8}\,O_3$ cathode degradation. J. Mater. Res. **27**, 1992–1999 (2012). https://doi.org/10.1557/jmr.2012.222
54. E.J. Crumlin, E. Mutoro, Z. Liu et al., Surface strontium enrichment on highly active perovskites for oxygen electrocatalysis in solid oxide fuel cells. Energy Environ. Sci. **5**, 6081–6088 (2012). https://doi.org/10.1039/C2EE03397F
55. E. Mutoro, E.J. Crumlin, H. Pöpke et al., Reversible compositional control of oxide surfaces by electrochemical potentials. J. Phys. Chem. Lett. **3**, 40–44 (2012). https://doi.org/10.1021/jz201523y